Proceedings of ASME Turbo Expo 2011
GT2011
June 6-10, 2011, Vancouver, British Columbia, Canada

GT2011-45503

NUMERICAL PREDICTIONS OF ROTATING STALL IN AN AXIAL MULTI-STAGE-COMPRESSOR

Dr Caetano Peng
Rolls-Royce Plc.
Fans SCU
Moor Lane Building ML-44 D2
PO Box 31 Derby
DE24 8BJ England
United Kingdom

ABSTRACT

This paper describes a numerical investigation of rotating stall in an axial multi-stage compressor using an in-house CFD (Computational Fluid Dynamics) based aeroelasticity code. This study investigates the effects of VSV (variable stator vanes) schedule on the occurrence of rotating stall at engine part-speed. Moreover, the effects of VSV circumferential mis-stagger angles (e.g. vane stagger angle variation) on the inception of rotating stall are also investigated. Virtual pressure probes are used here in the CFD models to extract unsteady pressure levels at locations of interest. These numerical studies have also enabled to evaluate the blade peak displacements due to rotating stall and hence to predict the blade vibration levels. In general, the numerical results would appear to be in line with past experience from rig and development engine data.

NOMENCLATURE

CFD	Computational Fluid Dynamics
FE	Finite Element
HCF	High Cycle Fatigue
FFT	Fast Fourier Transform
EO	Engine order
EO_K	Engine order from static frame of reference
EO_{SG}	Engine order from rotating frame of reference
Kulite	Unsteady pressure probes
n_{cell}	Number of stall cells
VSV	Variable stator vanes
Ω_{cell}	Speed of rotating stall cells
f	Modal frequency
fcell	Frequency of stall cells
f_K	Frequency measured by kulite probes
f_{rotor}	Frequency of shaft
f_{blade}	Frequency measured on blade

1. INTRODUCTION

Modern compressors tend to deliver high air mass flow and operate at the highest possible pressure ratios to increase their efficiency and overall performance. As rotor stages of the compressor reach higher points of their operating characteristics, the compressor tends to become more susceptible to occurrence of rotating stall and surge.

Rotating stall can be described as an aerodynamic phenomenon where small flow separations due to reduced flow rate have developed into relatively large cells (i.e. air pockets) known as stall cells or lobes that rotate about the compressor in the circumferential direction on a given rotor stage at a fraction of shaft rotational speed (i.e. usually varying from 30 to 70% of shaft rotational speed). If the forcing frequencies due to these stall cells coincide with blade natural frequencies then the blades can experience very high resonance stresses that could lead to high cycle fatigue blade failures. Moreover, this phenomenon can also have adverse effects on engine performance and increase engine noise levels.

Most compressors experience some rotating stall effects at certain engine operating conditions. Published literature [1-4] describes two types of rotating stall, the spike inception and modal stall inception respectively. The spike stall inception would appear to be the most common

one. It occurs due to a significant increase in the incidence angles of highly loaded rotors. Whereas, the occurrence of the modal stall inception is controlled by the gradient of the compressor pressure rise and mass flow characteristic. Effectively, rotating stall is strongly influenced by the compressor axial matching. The stall inception mechanism corresponding to the highest value of flow coefficient could be controlled by changing the axial matching of the compressor, either by re-setting the variable stator vanes or by adjusting the shaft speeds.

Rotating stall in axial multi-stage-compressors tends to occur at part-speeds particularly when operating at off-design conditions with extreme VSV (variable stator vanes) malschedule (note that this is not always the case, it can also occur at high speeds). These phenomena generate sometimes under certain operating conditions a relatively high number of stall cells close to the number of rotor blades with cells of small size (often less the half of blade span). However under different operating conditions, the rotating stall can result in a low number of cells that are large (sometimes covering the full blade span). The number of stall cells, their size and intensity vary with operating conditions such as shaft speed, aerodynamic flow conditions, variable vane schedule, tip running clearances, circumferential vane stagger angle variation, inlet air flow or downstream pressure field distortions, engine deterioration, etc. Note that the occurrence of the rotating stall does not always cause significant adverse effects on mechanical vibration, noise or aerodynamic performance of the compressor. If the formed stall cells are sufficiently large in size and generate sufficiently high-pressure perturbations then the presence of rotating stall can have detrimental effects on blade vibration, compressor efficiency and engine noise levels. Usually rotating stall phenomena are seen as a precursor to a compressor surge event (i.e. sudden occurrence of compressor reverse flow). It is important to note these phenomena tend to occur at off-design conditions for instance at part-speed or very high speeds.

Here the “spike type” rotating stall phenomena are classified into two subsets, “pseudo stall” and “rotating stall” respectively. The distinction between the two rotating stall cases is based on the number of stall cells, size, transient behaviour and levels of rotor blade forcing. The term “pseudo stall” is used herein to describe the rotating stall phenomena where the number of stall cells is relatively high (i.e. ~15 to 30 cells), cells rotating at about 60-70% of shaft speed and the blade vibration stress levels are usually relatively low. The “pseudo” stall cells tend to be highly transient; the cells can merge as well as break down into smaller cells under the same engine operating conditions. As the number of cells reduces and their size grows, their rotational speed tends to become low and if their forcing frequency matches the blade natural modal frequency then the blade could experience high resonance vibration responses. In contrast, the term “rotating stall” is used herein to describe the phenomena where the number of stall cells is relatively low (i.e. ~1 to 12 cells), cells rotating at fraction of shaft speed and because their forcing frequencies tend to be close to some of blade natural modal frequencies, they can potentially give rise to very high blade resonance stress levels. Schematic illustrations of part-span and full-span stall cells on a compressor rotor are shown in Fig.1.

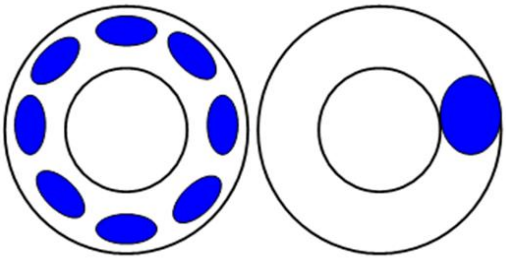

Figure 1 Schematic diagram of eight cells part span and one cell full span rotating stall.

Here, the conjecture from blade vibration response levels is that the increase in the number of stall cells is associated with the reduction of cell size. The occurrence of “rotating stall” is associated with relatively large size cells and small number of cells rotating at low fraction of shaft speed. Whereas the “pseudo stall” case is related to relatively small cells and a high number of stall cells rotating at a high fraction of shaft speed. The smaller these cells become the less adverse effects they have on the compressor.

1.1 Basic Rotating Stall Onset mechanisms

The operating points of individual stages of the compressor are strongly influenced by the change in axial matching of the flow field at off-design conditions [5]. The axial matching or “stage stacking” of the compressor defines how stage-operating points (i.e. pressure ratio and non-dimensional mass flow function) move relative to their individual design points. The effects of changes in stage operating points are cumulative and they affect the efficiency and the stability of the compressor.

The reduction in flow rate of an axial compressor at a constant shaft speed tends to increase the rotor and stator incidence angles. Moreover the increase in aerodynamic work input and diffusion of the flow leads to an increased pressure rise across the rotor stage or compressor. As the flow coefficient is reduced further, a critical point is reached beyond which the blade-to-blade flow field no longer can sustain the pressure rise across it. The existent quasi-steady flow field then becomes unstable and breaks down. This process is usually

accompanied by a sudden loss of pressure rise. This critical operating point at which the flow through the compressor becomes unstable is known as “stall point” and it defines the low flow limit of useful compressor work.

The stalling phenomena can occur at local scale and/or global level. On a global level, the stall can be regarded as instability of the whole compression system, which is highly influenced by the gradient of the compressor pressure rise and mass flow characteristic. On the other hand on a local scale, the stall is a breakdown of the blade-to-blade flow field into stall cells, which subsequently could lead to the occurrence of surge events. When the compressor operating point is pushed beyond its stability limit, the flow field breaks down into a number of rotating stall cells. The two onset-rotating stall mechanisms often reported are the “modal” and “spike” stall inception. The modal mechanism of stall inception is characterised by a circumferentially varying velocity field, which rotates in the direction of rotor at about 30%-60% of rotor speed. Fig.2 shows a schematic diagram of a first order mode.

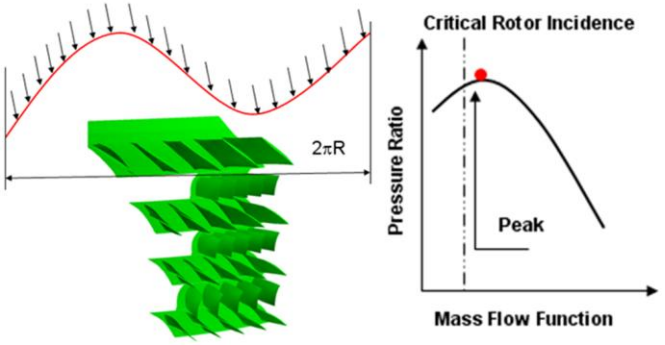

Figure 2 Schematic diagram of first order mode (one wavelength per circumference).

As shown in Fig.2, when the compressor stalls with a modal mechanism, the slopes of the overall compressor characteristics are approximately zero at stall point. The first order mode or one wavelength per circumference is the most commonly seen. However second order and high order modes have also been observed experimentally [1] and [6]. The wavelength of the modal wave is much longer than the blade pitch and the modal wave is therefore described as a “long scale” disturbance. The velocity perturbation is seen axially throughout all stages of the compressor. There is very little span-wise velocity variation; the disturbance is mainly two-dimensional, axial and circumferential respectively. The modal perturbation increases rapidly in amplitude from originally very small disturbance as the compressor flow coefficient is reduced at a given compressor aerodynamic speed. It is interesting to note that [7] developed a theoretical foundation for the modal structure before the experimental observations by [8]. The “spike” stall inception is described as a finite stall cell, which in its infancy phase affects the flow in only one or two blade passages and over part-span. Because the size of the cell is approximately the blade pitch, this phenomenon is described as a “short length scale” disturbance. Usually in low and intermediate pressure compressors, “spike” stall inception is seen in the first rotor. However, [5] reported that the occurrence of “spikes” in downstream bladerows as well in low speed compressors. Fig.3 illustrates local region of flow separation associated with “spike” stall inception.

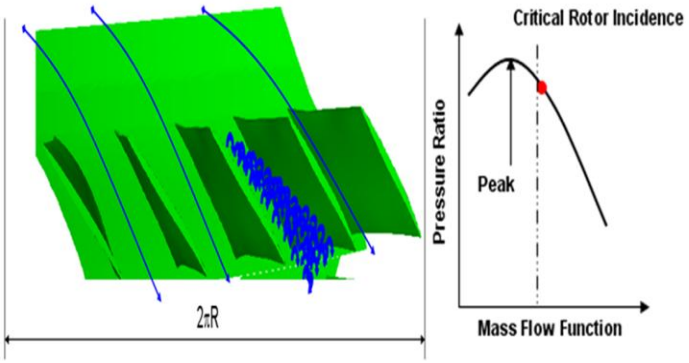

Figure 3 Schematic diagram shows small region of separated flow associated with “spike” stall inception.

The separated flow region in the “spike” stall inception gives rise to “spikes” in the measured velocity and pressure traces. [1-4] and [9] have shown that the “spike” stall inception begins with the breakdown of the flow field in a single-bladerow. When stall is triggered by “spike” mechanism, the overall characteristics have a negative gradient at stall as shown in Fig.3. Since the physical scale of “spike” inception is much smaller than the scale at which the characteristics are measured, it is possible for the slope of individual blade passages to become positive and the flow in this passage to become unstable (i.e. initiation of “spike” stall) while the overall slope of the overall compressor characteristic was still negative. In low speed compressors, “spike” stall inception occurs often in front stages, particularly rotor 1 because of the rate of increase in rotor 1 incidence near stall. Effectively, the rotor 1 incidence angle increases more quickly near stall than the incidence angle of the downstream rotor stages. The formation of “spikes” at rear stages can occur when operating at high shaft speeds. This should be expected since the axial matching of the compressor at high speeds causes the rear stages to operate at higher incidences than the front and middle stages. In contrast, the development of a modal disturbance is associated with instability of the flow throughout the whole compressor. The effects of axial matching on the stall inception are consistent with experimental results from high-speed compressor tests [9].

1.2 Evidence of Rotating stall Occurrence

This paper pays particular attention to "spike type" rotating stall phenomena (described here as "pseudo or rotating stall") that have been detected in low pressure, intermediate pressure and high pressure compressors. Both rotating stall and pseudo stall have been seen in engines and rigs. Rotating stall phenomena tend to occur usually when the compressor is operating under extreme VSV malschedule conditions or when the rotor or compressor is operating above its nominal working line. The number of stall cells can be determined from engine or rig tests using measured vibration responses from instrumentation (i.e. unsteady pressure probes, tip-timing probes, accelerometers or strainguages) mounted on both fixed (e.g. casing or stator vanes) and rotating frames of reference. Illustrations of rotating stall detection using unsteady pressure probes (kulite probes) and strain gauges are shown in Figs. 4 and 5.

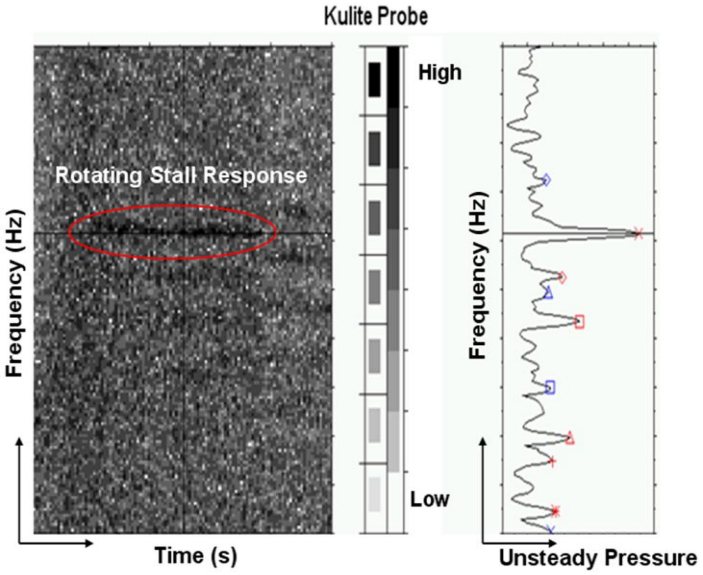

Figure 4 Detection of rotating stall using kulite probes.

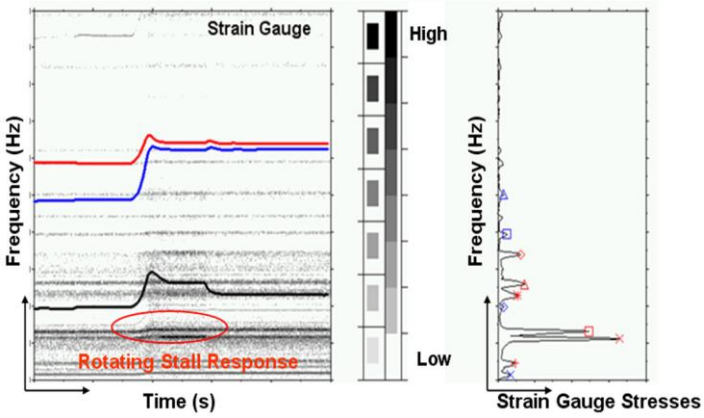

Figure 5 Detection of rotating stall using strain gauges.

The responses highlighted in Figs. 4 and 5 have been identified as due to rotating stall and they were captured simultaneously by both Kulite probes (unsteady pressure sensors) mounted on engine casing and strain gauges on the rotor blade. These plots are also given as a function of engine shaft speed rather than time. Once known the speeds of occurrence of Kulite probes and strain gauge responses, the vibration engineers can extract the response frequencies, response levels and engine orders (EO, response frequency divided by shaft speed).

The number of stall cells or lobes is just a sum of engine orders observed from fixed (i.e. casing or stator) and rotating (i.e. rotor) frames of reference respectively.

$$n_{cell} = EO_K + EO_{SG} \quad (1)$$

$$f_{cell} = \frac{f_K}{n_{cell}} \quad (2)$$

$$\%\Omega_{cell} = \frac{f_{cell}}{f_{rotor}} 100\% \quad (3)$$

The blade forcing frequency at resonance under rotating stall-forcing conditions can be calculated using the following expression:

$$f_{blade} = n_{cell} \times (f_{rotor} \pm f_{cell}) = n_{cell} \times f_{rotor} \pm f_K \quad (4)$$

Alternatively, the relative speed of stall cells can be calculated as the gradient of pressure pulses from circumferential pressure probe positions and unsteady pressure versus time histories. Note that "pseudo stall" and "rotating stall" are effectively all rotating stall phenomena. The classification given herein is just an arbitrary distinction based on the number of lobes, transient nature of the cells and intensity of responses.

2. ANALYSIS METHODOLOGY

The work discussed here is based on CFD studies on an eight-stage compressor with seventeen bladerows. The compressor model contains three-variable-stator-vane-stages and all rotors have nominal blade tip running clearances. The first six vibration modes from FE analyses are included in the rotating stall simulations. The aeroelasticity simulations are performed using an in-house aeroelasticity suite named AU3D. This CFD based tool allows computations of both steady-state-solution and unsteady flow computations. Aerodynamic boundary conditions, shaft speed, VSV schedule and malschedule are chosen to simulate some worst conditions that this compressor could experience at engine part-speeds.

In order to obtain blade modal properties, the FE computations are performed first to determine the natural frequencies and modeshapes of the vibration modes of interest using Campbell diagrams. Then CFD steady-state-solution simulations are performed on single-blade-passage-one-bladerow, whole-compressor-single-blade-passage and hybrid-passage-multi-bladerow models (full-annulus-&-single-blade-passage-multi-bladerow models). The solutions from steady-state-flow computations are then used as starting solutions in the unsteady-flow simulations. The unsteady-flow rotating stall computations are performed on full-assembly-multi-bladerow models. Both steady-state-solution and unsteady-flow simulations included the effects of nominal (design) blade tip running clearances. Moreover, the effects of flow incidence are investigated by conducting compressor analyses with reference variable vane schedule (stages 1-3 VSV rotated to pre-selected angular positions) and extreme vane malschedule where each individual VSV stage is either open or closed up to about 3^o. The compressor operates with high flow incidences at part-speeds because the VSVS are more closed. Note that the reference VSV schedule here is a non-optimised schedule.

The unsteady-flow results are then processed to assess whether rotating stall is present or not. This assessment is by evaluating the unsteady pressures and their frequency contents, performing flow visualizations close to rotor of interest and by analysing the contents of aerodynamic modal force histories. Once identified the aerodynamic modal forces associated with rotating stall, these can be converted into blade peak modal displacement by applying the appropriate damping values. The vibration stresses are then calculated basing on peak displacements and FE analyses. Then, one should be able to evaluate the strength of rotating stall in terms of blade vibration stress levels.

2.1 AU3D Suite

The basic aeroelasticity suite comprises of AU3D CFD based aeroelasticity code, SC03 FE analysis tool and FORSE multi-harmonic balance forced response program. This system is illustrated in Fig.6.

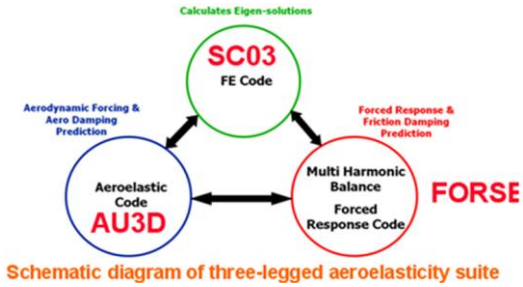

Figure 6 An in-house aeroelasticity suite.

FORSE is not used in the computations described herein. SC03 FE code is used to compute the natural vibration frequencies and modeshapes of vibration modes that are then interpolated onto CFD grids for the unsteady flow rotating stall simulations. The AU3D main solver is 3-D Reynolds averaged Navier-Stokes equations based code that uses a time-marching scheme. The description of AU3D code can be found in the references [10, 11, 12 and 13]. The aeroelasticity suite in Fig.6 has been used over a wide range of applications. Accuracy of computational methods and some validation of the code used herein can be found in [14, 15].

2.2 Models and Boundary Conditions

The compressor investigated herein is an eight-stage intermediate pressure compressor comprising seventeen bladerows of stators and rotors. A single-blade-passage-one-bladerow CFD model consists of about three hundreds thousands cells. The single-blade-passage-whole-compressor CFD mesh has approximately five millions cells. This model is illustrated in Fig.7.

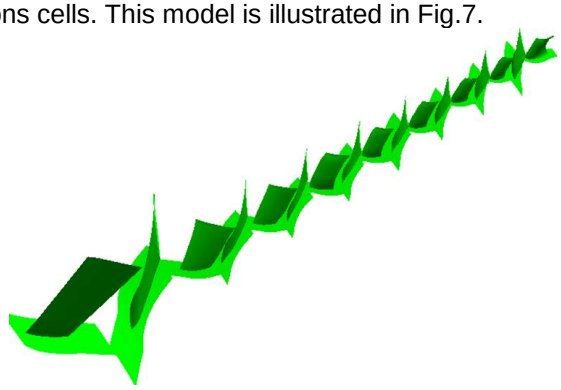

Figure 7 Single-blade-passage-compressor CFD grid.

The unsteady flow rotating stall model of about hundred million cells is shown in Fig.8.

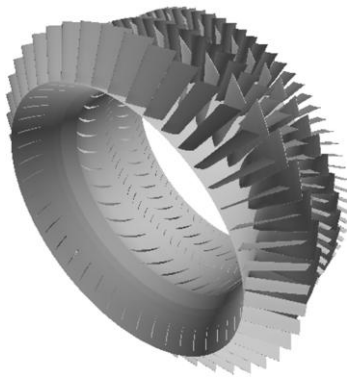

Figure 8 Full-annulus-multi-bladerow model.

The effects of VSV are investigated by performing steady-state-solutions with reference VSV schedule and $\pm 3^o$ unganged VSV malschedule (unganged means that

there is no proportionality between angular settings of VSV stages and malschedule means the VSV angles are set to be off reference VSV schedule). The solutions from these computations are then used in unsteady flow rotating stall computations. The analysis speed is set to represent the engine part-speed (60-85% of shaft speed) conditions. The aerodynamic boundary conditions are based on engine part-speed conditions. These are first obtained from through-flow computations. Then the inlet (total pressures) and exit (static pressures) individual bladerow boundary conditions extracted from the through-flow computations are used as initial boundary conditions in AU3D steady-state-solution simulations. Note that initial aerodynamic boundary conditions from the through-flow computations can be applied to a single-bladerow or to the whole compressor model. In either case, they are applied as inlet and exit boundary conditions on single-blade-passage model or as inlet boundary conditions for the first bladerow and exit boundary conditions for the last bladerow of the whole compressor model.

The modeshapes used in rotating stall simulations are obtained from FE rotor analyses. Preliminary assessment of vibration modes shows that the modeshapes obtained from FE blade alone model and FE bladed-disc model have negligible differences. Therefore, only modeshapes of FE blade alone model are used in the computations.

3. RESULTS AND DISCUSSIONS

3.1 Steady-State-Solution Results

The steady-state-flow-solution computations are done on single-blade-passage-single-bladerow models, whole-compressor-single-blade-passage and hybrid-passage-multi-bladerow models. An example of steady-state-solution analyses on hybrid-passage-multi-bladerow model is shown in Fig.9.

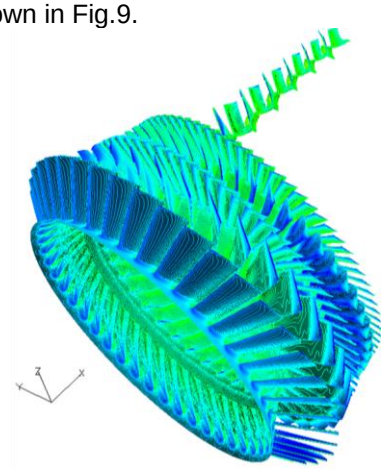

Figure 9 Plot of axial flow velocity of the hybrid model.

The results from steady-state-solution computations show the sensitivity of compressor flow at analysis speed to unganged VSV malschedule. Here, the unganged malschedule is defined as more open or more closed VSV relative to the reference VSV schedule. The plot of axial flow velocity for the reference VSV schedule, about 3^o closed VSV schedule and about 3^o open VSV schedule case studies are shown in Fig.10.

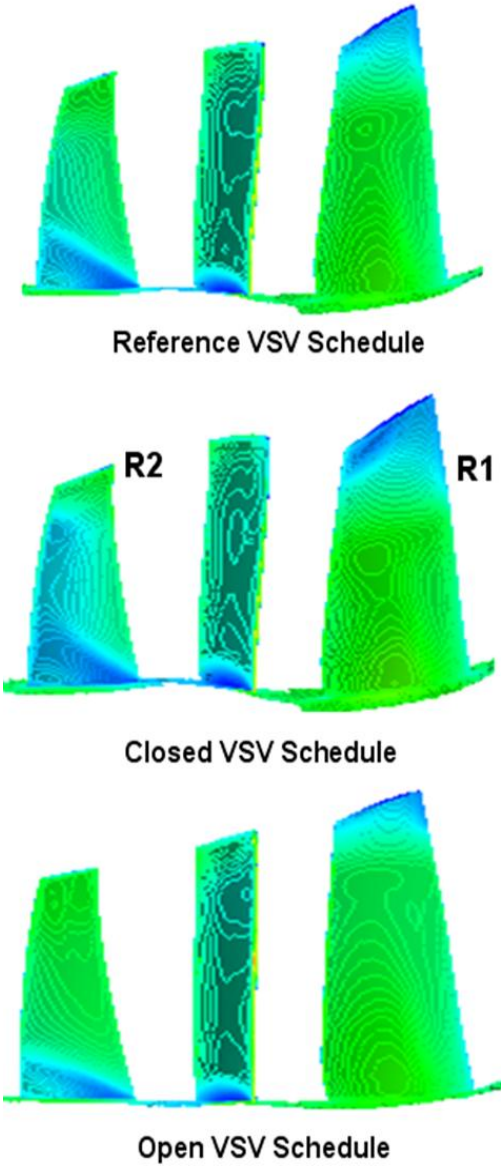

Figure 10 Plot of axial flow velocity for three case studies of VSV schedule.

As can be seen in Fig.10, small flow separations are seen at the blade tip of the first rotor and close to blade hub region of the second rotor. These stall regions would indicate that the first rotors are most sensitive at this given speed. By closing VSV by about 3^o relative to the reference VSV schedule, the flow separations worsen for the first two rotor stages. In contrast by opening the VSV

by about 3° relative to reference VSV schedule, the blade tip and hub stall regions diminish relative to the reference VSV schedule. The flow separations or stall regions expressed in terms of rotor exit axial velocity along blade span can be seen in Figs.11 and 12.

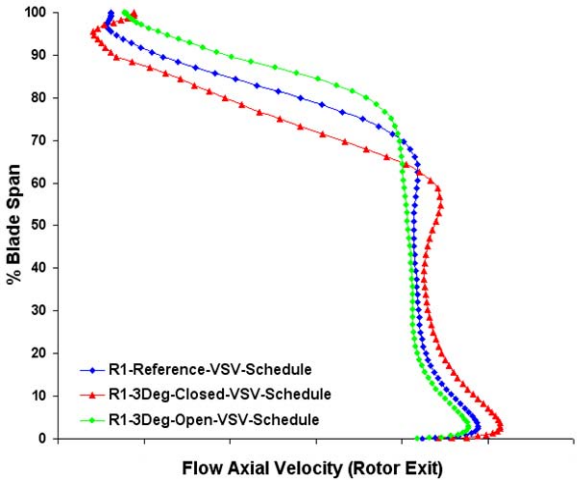

Figure 11 Plot of rotor 1 exit axial flow velocity for three case studies of VSV schedule.

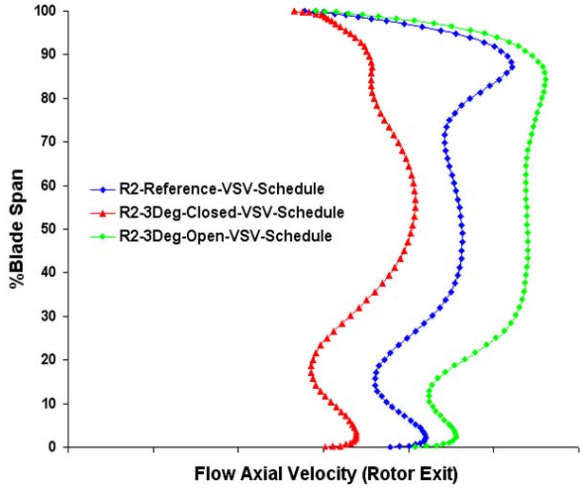

Figure 12 Plot of rotor 2 exit axial flow velocity for three case studies of VSV schedule.

As shown in Figs.11 and 12, the flow profiles of rotors 1 and 2 worsen for the case of closed VSV schedule while they tend to improve with the open VSV schedule case. The VSV sensitivity studies indicate that the reference and 3° closed VSV schedules shown in Figs.10, 11 and 12 are mostly likely to be prone to rotating stall. This should be confirmed through unsteady flow rotating stall simulations. It has been said before that the steady-state-flow-solution computations cannot be used to assess qualitatively the propensity of compressors at a given speed to rotating stall. However the present results indicate that the steady-state-solution could be used to assess qualitatively the likelihood of occurrence of rotating stall by investigating the rotor stall regions and rotor stage characteristics. It should be pointed out that these steady-state simulations would not be accurate in predicting the likelihood of occurrence of rotating stall and would not tell the unsteady pressure and blade amplitude levels due to rotating stall.

3.2 Unsteady Flow Results & Discussions

The unsteady flow rotating stall simulations are performed on full-assembly-multi-bladerow models using the aero boundary conditions and starting solutions obtained from converged steady-state-solution computations. Relevant vibration modeshapes from FE analyses are included in these rotating stall simulations. Three sets of analyses are considered:

a) Reference VSV schedule (non-optimised VSV schedule) model and ±3° unganged VSV malschedule applied to reference VSV schedule model;
b) Investigation of the effects of circumferential vane stagger angle variation on rotating stall responses for ±3° unganged VSV malschedule applied to reference VSV schedule model;
c) Modified VSV schedule model (VSV stages are open or closed accordingly relative to reference VSV schedule to prevent or reduce rotating stall responses by unloading the rotor of concern) and ±3° unganged VSV malschedule applied to modified VSV schedule model.

Random circumferential vane stagger angle variation of ±0.5° is applied to sets (a) and (c). The computations for set (b) are performed using three levels of random vane stagger angle variation, ±0.5°, ±1.5° and ±3.0° respectively. Note that the random circumferential vane stagger angle variation was applied to the first stage of VSV to help triggering the occurrence of rotating stall. It would take a long time to initiate rotating stall in a symmetrical system by small inherent computational numerical variations. Application of random pattern circumferential vane stagger angle variation is more akin to a real system because it introduces non-axisymmetries and accelerates the initiation of rotating stall in flows prone to stall.

The analyses allow us to extract the unsteady flow parameters (basic unknowns) as well as aerodynamic modal forces applied to blade surfaces. Then for known damping parameters (total modal damping), the modal forces can be converted into peak blade displacements and subsequently converted to vibratory stresses and stress ratios (applied vibratory stress over modal fatigue strength) by assuming they are at resonance. Six numerical or virtual kulite probes are placed

circumferentially 60^{o} apart at inlet and exit surfaces of the stators and rotor (about half axial distance between stator and rotor at about 75%-85% blade span) to monitor unsteady pressures and to determine the stall cells rotational speed. A schematic diagram of virtual probes is shown in Fig.13.

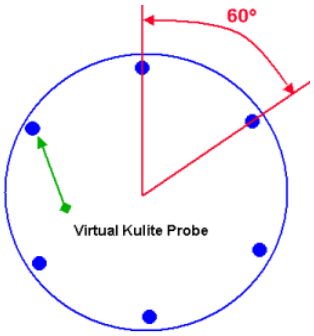

Figure 13 Circumferential positions of virtual kulite probes.

Plot of circumferential pressure probe positions and unsteady pressure versus shaft revolutions histories for the reference VSV schedule model indicates the occurrence of rotating stall, see Fig.14. The stall cells are rotating at about 69% of shaft speed. The number of stall cells and their rotation speed are in line with past test data. This speed is derived from the plot in Fig.14.

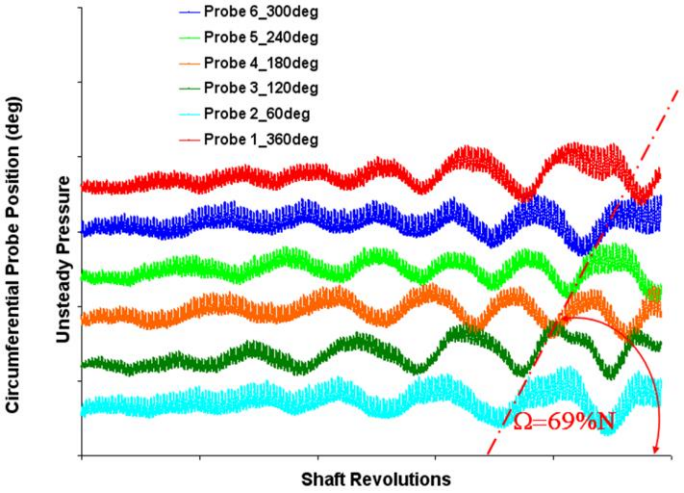

Figure 14 Virtual kulite pressure histories for the reference VSV schedule.

During the computations, the number of stall cells present in the flow would appear to be varying by mergence and splitting of existent cells until eventually settling to a fixed number after some engine revolutions. Fig.15, plot of unsteady static pressure at inlet surface of the rotor (about half way between the rotor and upstream VSV) shows clearly the stall cells. The number of relatively large stall cells is 10 but the small ones can be counted up to 17.

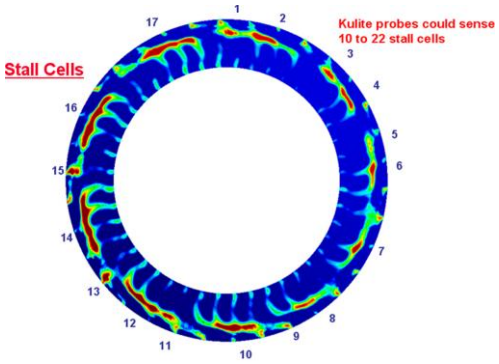

Figure 15 Rotor inlet surface static pressure view of stall cells for the reference VSV schedule.

The frequency components present in the flow during the rotating stall can be extracted by performing an FFT of the virtual kulite unsteady pressure histories. Then, the plots of unsteady pressure versus frequency can be expressed in terms of engine order (EO) by dividing the frequencies by the shaft speed. Figs.16 shows plots of unsteady pressure versus EO.

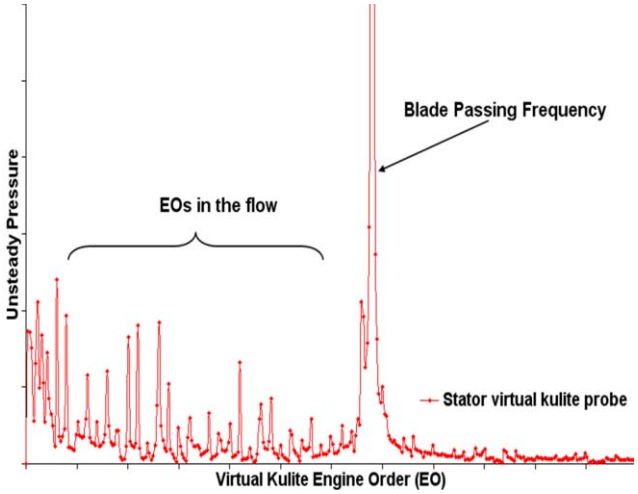

Figure 16 Virtual kulite probe unsteady pressure versus EO plot.

Note that not all EOs shown in Fig.16 are due to rotating stall. Some are just blade passing frequencies and others are due to circumferential vane stagger angle variations. The largest peak response shown in Fig.16 is due to blade passing frequency.

Signs of rotating stall presence can also be detected from modal force histories and their FFT plots. Figs.17 and 18 show plots of modal force histories and Fourier coefficients for reference VSV schedule and ± 3.0^{o} unganged VSV malschedule on reference VSV schedule. Both VSV schedule cases indicate the presence of rotating stall. However, the intensity of rotating stall in terms of aerodynamic modal forces would appear to

increase quite significantly with increase in VSV malscheduling.

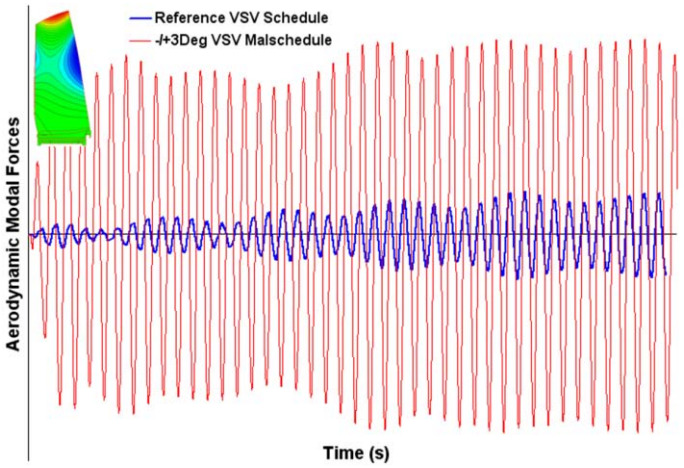

Figure 17 Predicted modal force histories for reference VSV schedule and $\pm$ 3.0^o unganged VSV malschedule.

The modal forces shown here are calculated for second flap (second flexural) vibration mode of the rotor of interest. This mode is chosen just for illustration since other vibration modes also experience responses due to rotating stall. As can be seen in Fig.18, both non-integral forcing due to rotating stall and EO forcing components are present in the flow. The EO forcing component is due to circumferential vane stagger angle variation. In the absence of rotating stall, only integral EO forcing would be present.

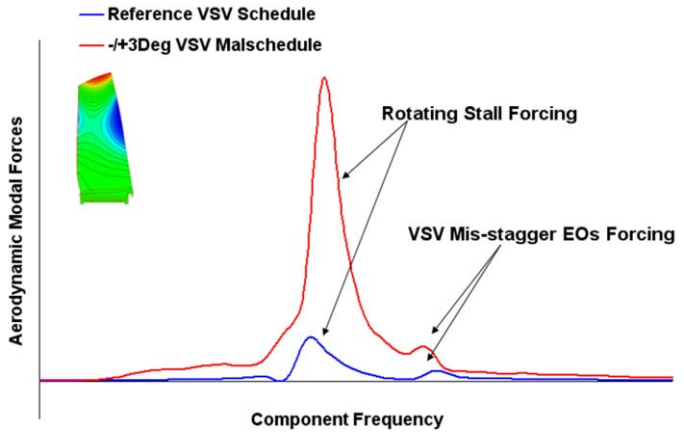

Figure 18 FFT of predicted force histories for reference VSV schedule and $\pm$ 3.0^o unganged VSV malschedule.

The effects of circumferential vane stagger angle variation on rotating stall responses are investigated here by performing analyses for $\pm$3^o unganged VSV malschedule applied to reference VSV schedule model. These analyses should help to evaluate whether the vane stagger angle variation affects both non-integral and EO forcing components or just only non-integral forcing components. Plots of predicted modal force histories and FFT frequency components for second flap vibration mode are shown in Figs. 19 and 20 below.

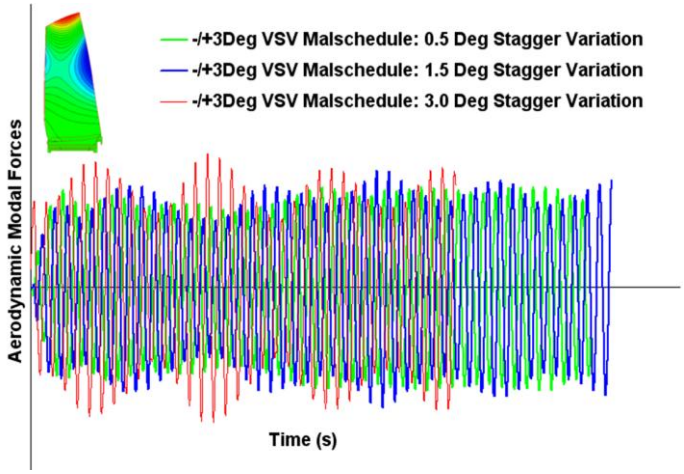

Figure 19 Effects of circumferential vane stagger angle variation on rotating stall modal force histories.

As shown in Fig.19, the aerodynamic modal forces resulting from different levels of vane stagger angle variation would appear to be all of similar magnitude. However, Fourier components of modal forces shown in Fig.20 indicate clearly that integral EO forcing components are sensitive to vane stagger angle variation; the higher is the magnitude of stagger angle variation, the higher is the EO forcing due to circumferential vane stagger angle variation. The interesting feature to note from Fig.20 is the modal force amplitude due to rotating stall appears to be insensitive to vane stagger angle variation.

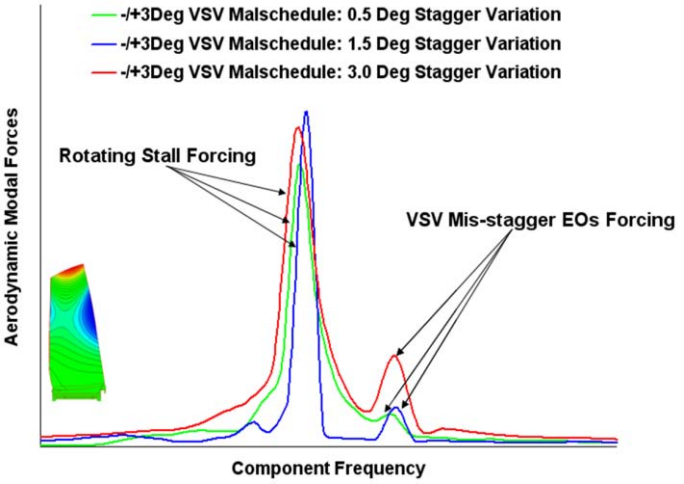

Figure 20 Effects of circumferential vane stagger angle variation on rotating stall component modal force histories.

It would be interesting to assess whether the rotating stall numerically triggered by vane stagger angle variation would still be present after removal of circumferential vane stagger angle variation. The results from this study are summarized in Fig.21.

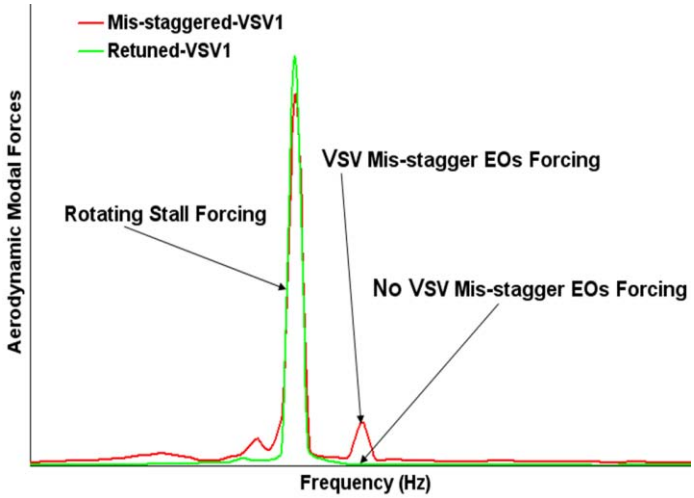

Figure 21 Effects of removal of circumferential vane stagger angle variation after initiation of rotating stall.

As can be seen in Fig.21, the amplitude of modal forces due to rotating stall are about the same before and after the removal of circumferential vane stagger angle variation used to trigger the rotating stall in the first place. However, the forcing component resulting from VSV mis-stagger EOs disappears with the removal of circumferential vane stagger angle variation (plot shown in green in Fig.21). This is an important finding that indicates the random patterns of circumferential vane stagger angle variation and even its magnitude may not be important once the rotating stall is initiated.

Rotating stall simulations are also performed here on modified VSV schedule and $\pm 3^{o}$ unganged VSV malschedule (on modified VSV schedule) models with a view to prevent or reduce rotating stall responses. These analyses are to show numerically that VSV schedule can potentially be used as a means to controlling rotating stall responses since it is known experimentally to be the case. This is done by changing the VSV angular settings both in terms of absolute angles and configuration. However, VSV optimization for rotating stall could be difficult to apply over a wide engine speed range and it could also have some undesirable side effects. The shaft speed, aerodynamic boundary conditions and mechanical models (FE) are exactly the same as those used for reference VSV schedule models. Plot of circumferential pressure probe positions and unsteady pressure versus shaft revolutions histories for the modified VSV schedule model is shown in Fig.22.

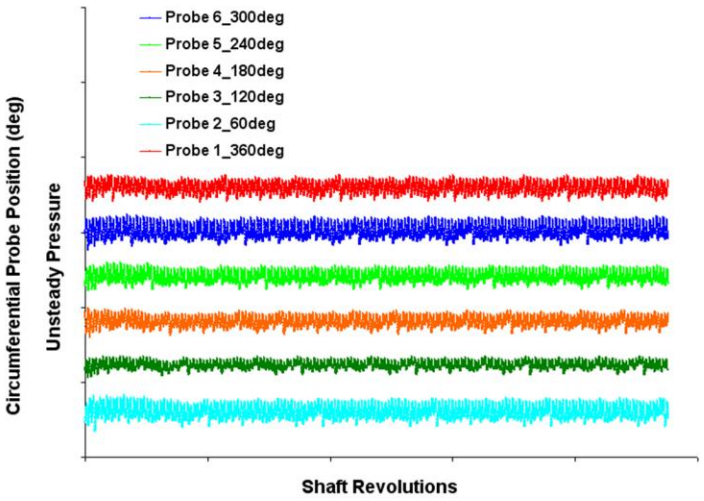

Figure 22 Virtual kulite pressure histories for modified VSV schedule.

One could compare the virtual kulite pressure histories shown in Figs.14 and 22. As can be seen in Fig.22 unlike Fig.14, there is no rotating stall presence in the flow. This conclusion is also evidenced in Fig.23 by comparisons of unsteady pressure plots between the reference VSV schedule and modified VSV schedule cases. Plot of unsteady pressure at inlet surface of the rotor in Fig.23 shows no stall cells for the modified VSV schedule case.

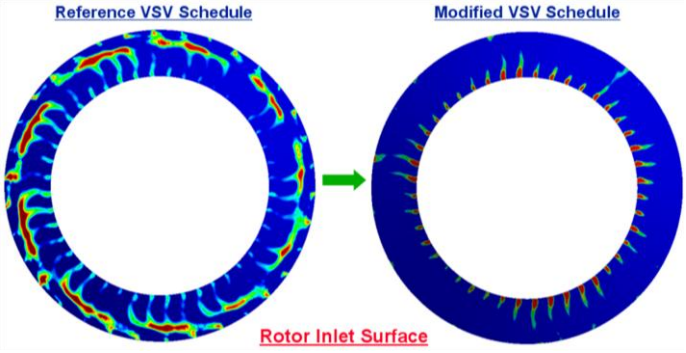

Figure 23 Rotor inlet surface unsteady static pressure iso-contours views of stall cells for reference and modified VSV.

The non-occurrence of rotating stall for the modified VSV schedule case is because this schedule reduces the stage loading and moves away from the rotating stall onset region on stage characteristic of the susceptible rotor.

The rotating stall phenomena re-occur when $\pm 3^{o}$ unganged VSV malschedule is applied onto the modified VSV schedule model. However as shown in Fig.24, the modal forces are lower than those for the reference VSV schedule. These low modal forces can also be seen in the FFT plots in Fig.25. Plots of aerodynamic modal forces in

Figs.24 and 25 are to reiterate the role of VSV schedule in controlling the rotating stall and to show the significance of the design VSV schedule which in time will become malschedule due to engine service deterioration.

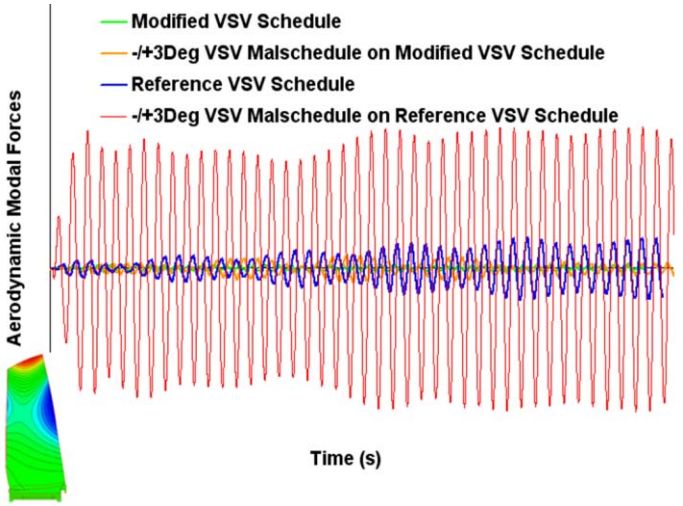

Figure 24 Comparisons of predicted modal force histories for different types of VSV schedules.

Figure 25 shows that only the EO forcing component is present for the modified VSV schedule. The $\pm 3^{o}$ unganged VSV malschedule on modified VSV schedule case shows lower modal forces (due to rotating stall) than the reference VSV schedule and $\pm 3^{o}$ unganged VSV malschedule on reference models. These differences are likely to be due to changes in the stage loading of the front rotors with changes in VSV schedules at engine part-speeds (60-85% of shaft speed).

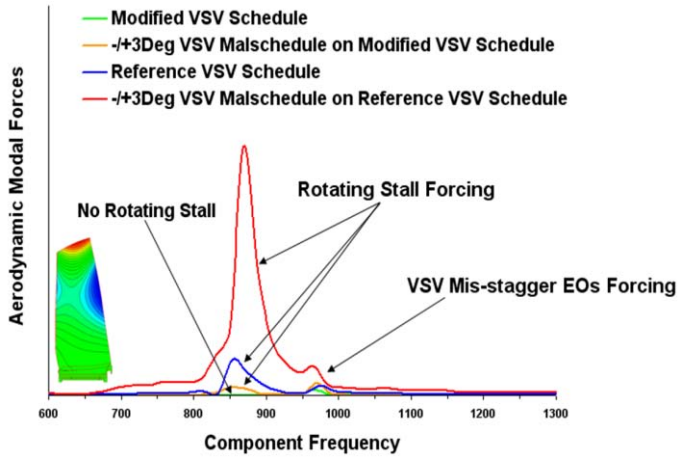

Figure 25 No rotating stall for modified VSV schedule.

Note that the EO forcing component appears to increase with the increase in the levels of VSV malschedule but not as much as rotating stall forcing. Once the aerodynamic modal forces and modal damping are known, one can calculate the actual blade vibratory stresses resulting from rotating stall forcing and hence the stress ratios or modal endurances.

The last case study is an attempt to simulate the effects of VSV changes on rotating stall in real-time. A "pseudo transient" response study is performed here where the rotating stall is initiated on unganged VSV malschedule and then once been developed, the VSVs are rotated to a different schedule (using the same CFD grid by mesh morphing) to eliminate rotating stall. Here, the analysis with the new VSV schedule is a continuation of a CFD flow solution with rotating stall. The results of this computation expressed in terms of aerodynamic modal forces are shown in Fig.26.

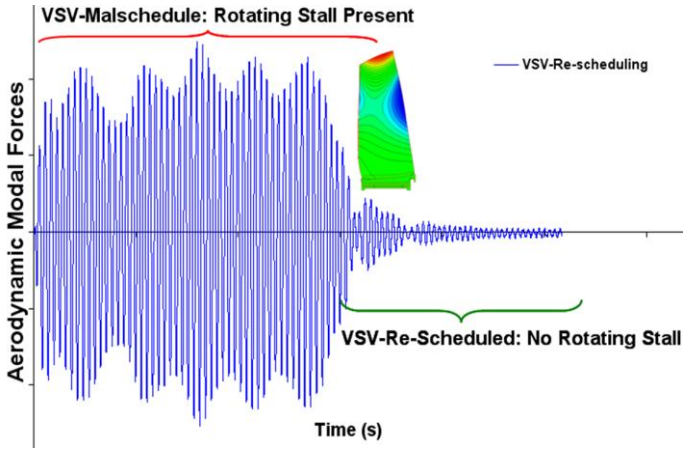

Figure 26 Reduction of rotating stall aerodynamic modal forces due to changes of VSV schedule in a continued CFD analysis.

As can be seen in Fig.26, high aerodynamic modal forces are seen during rotating stall and then when the VSVs are rotated, these modal forces are significantly reduced due to absence of rotating stall. This study shows that the numerical tools have the potential to performing real-time flow simulations of VSV changes.

4. CONCLUSIONS

Unsteady flow rotating stall simulations performed here have shown that the "spike type" rotating stall in axial compressors can be predicted using CFD tools. The VSV schedule is an important factor to rotating stall and compressor stability. This study shows the occurrence of rotating stall for a non-optimised VSV schedule (reference VSV schedule) and for excessive unganged VSV malschedule. The rotating stall responses tend to increase with increasing levels of VSV malscheduling. Moreover, the effects of random circumferential vane stagger on rotating stall have also been investigated here. The simulations indicate that aerodynamic modal forces due to rotating stall are insensitive to levels of vane

stagger angle variations. However, the EO forcing component due to vane stagger angle variation is sensitive to the levels of random vane stagger angle variation. An increase in the levels of vane stagger angle variation equates to an increase in EO forcing component. The rotating stall computation is able to sustain the rotating stall after the removal of circumferential vane stagger angle variation used to trigger the rotating stall in the first place. Moreover, a "pseudo transient" response case study performed here shows that the numerical tools have the potential to performing real-time flow simulations of VSV changes.

Here, the numerical investigations have also shown that rotating stall responses can be prevented or reduced by optimising the VSV schedule. The unsteady flow computations included modeshapes from FE analyses for calculation of aerodynamic modal forces. Knowing the modal forces due to rotating stall and modal damping, the blade peak displacements, vibratory stresses and stress ratios or modal endurances can all be computed for the assessment of blade HCF responses.

5. ACKNOWLEDGMENTS

The author would wish to thank Rolls-Royce plc for allowing this publication. Moreover, the author would wish also to express special acknowledgments to Dr Mehdi Vahdati from Imperial College London for his valuable technical inputs.

6. REFERENCES

[1] Day, I. J., "Active Suppression of Rotating Stall and Surge in Axial Compressors", Trans. ASME, Journal of Turbomachinery, Vol.115, pp.40-47 1993.

[2] Day, I.J., "Review of Stall, Surge and Active Control in Axial Compressors", 11th ISABE Conference, Tokyo 1993.

[3] Day, I.J., "Stall Inception in Axial Compressors", Trans. ASME Journal of Turbomachinery Vol.115, pp.1-9, 1993.

[4] Day, I.J., "Instabilities and Separations in the Deverson Compressor" Rolls-Royce report DNS12063, 1994.

[5] Camp, T.R., *Aspects of the Off-Design Performance of Axial Flow Compressors,* PhD Dissertation, Department of Engineering, University of Cambridge 1995.

[6] Paduano, J., Epstein, A.H., Valavani, L., Longley, J.P., Greitzer, E.M. and Guenette, G.R., "Active Control of Rotating Stall in Low Speed Axial Compressors", Trans. ASME Journal of Turbomachinery Vol.115, pp.48-56 1993.

[7] Moore, F.K. and Greitzer, E.M., "A Theory of Post-Stall Transients in Axial Compressor Systems: Parts I and II", Trans. ASME, Journal of Engineering for Power, Vol.106, pp.313-336 1986.

[8] McDougal, N.M., Cumpsty, N.A. and Hynes, T.P., "Stall Inception in Axial Compressors", Trans. ASME, Journal of Turbomachinery, Vol.112, pp.116-125, 1990.

[9] Wilson, A.G. and Freeman, C. "Stall Inception and Development in an Axial Flow Aero Engine", Trans. ASME, Journal of Turbomachinery, Vol.116, no.2. pp.216-225, 1993.

[10] Vahdati, M. and Imregun, M., "Non-linear aeroelasticity analyses using unstructured dynamic meshes", Proc. Instn. Mech. Engrs., Part C, Journal of Mechanical Engineering Science, 1996, **210** (C6), 549-564.

[11] Sayma, A. I., Vahdati, M., Sbardella, L. and Imregun, M., "Modelling of Three-Dimensional Viscous Compressible Turbomachinery Flows Using Unstructured Hybrid Grids", AIAA Journal, Vol.38, No.6, June 2000, 945-954.

[12] Sayma, A.I., Vahdati, M. and Imregun, M., "Multi-bladerow fan forced response predictions using an integrated three-dimensional time-domain aeroelasticity model", Proc. Instn. Mech., Engrs., Vol.214, Part C, IMechE 2000, 1467-1483.

[13] Vahdati, M., Sayma, A.I., Lee, S.J. and Imregun, M., "Multi-bladerow Forced Response Predictions for a Rig with Articulated Inlet Guide Vanes", In Proceedings of the National 4th High Cycle Fatigue Conference, Monterey, USA, 1999.

[14] Vahdati, M., Simpson, G. and Imregun, M., "Aeroelastic Behaviour of Aero-engine Core Compressors during Rotating Stall and Surge", Proceedings of ASME Turbo Expo 2006, May 8-11, 2006, Barcelona, Spain, ASME Paper GT2006-90308.

[15] Choi, M., Vahdati, M. and Imregun, M., "Effects of Fan Speed on Rotating Stall Inception and Recovery", Proceedings of ASME Turbo Expo 2010, June 14-18, 2010 Glasgow, UK.